Study of the departures from LTE in the unevolved stars infrared spectra

S Korotin, S Andrievsky, E Caffau, P Bonifacio, E Oliva

Monthly Notices
of the
ROYAL ASTRONOMICAL SOCIETY

MNRAS **496,** 2462–2473 (2020)
Advance Access publication 2020 June 17

doi:10.1093/mnras/staa1707

Study of the departures from LTE in the unevolved stars infrared spectra

S. A. Korotin,[1]★ S. M. Andrievsky,[2,3] E. Caffau,[3] P. Bonifacio[3] and E. Oliva[4]

[1]*Crimean Astrophysical Observatory, Nauchny 298409, Republic of Crimea*
[2]*Astronomical Observatory, Odessa National University, Shevchenko Park, UA-65014 Odessa, Ukraine*
[3]*GEPI, Observatoire de Paris, PSL Research University, CNRS, Place Jules Janssen, F-92195 Meudon, France*
[4]*INAF–Osservatorio Astrofisico di Arcetri, Largo E. Fermi 5, I-50125 Firenze, Italy*

Accepted 2020 May 13. Received 2020 May 13; in original form 2020 April 10

ABSTRACT

We present a study of departures from Local Thermodynamic Equilibrium (LTE) in the formation of infrared (IR) lines of Na I, Mg I, Al I, S I, K I, and Sr II in unevolved stars of spectral types F, G, K and metallicities around the solar metallicity. The purpose of this investigation is to identify lines of these species that can be safely treated with the LTE approximation in the IR spectra of these types of stars. We employ a set of 40 stars observed with the GIANO spectrograph at the 3.5 m Telescopio Nazionale Galileo and previously investigated by Caffau et al. We were able to identify many lines that can be treated in LTE for all the above-mentioned species, except for Sr II. The latter species can only be studied using three lines in the *J* band, but all three of them display significant departures from LTE. With our small-size, but high-quality sample, we can determine robustly the trends of the abundance ratios with metallicity, confirming the trends apparent from a sample that is larger by several orders of magnitude, but of lower quality in terms of resolution and S/N ratio.

Key words: line: formation – line: profiles – Sun: abundances – stars: abundances – stars: solar-type – Galaxy: evolution.

1 INTRODUCTION

With the advent of *Gaia* and especially the *Gaia* data release 2 (DR2; Arenou et al. 2018; Gaia Collaboration 2018) our vision on the Milky Way has changed: our Galaxy revealed to be bigger, the stars on average are more distant from the Sun than what we thought. For example, the classical vision we had of the Galactic halo formed by old, metal-poor, '*in situ*' stars has changed: this extended Galactic component is likely populated by stars accreted in a major event (see e.g. Belokurov et al. 2018; Haywood et al. 2018; Helmi et al. 2018; Di Matteo et al. 2019). However, the kinematics alone is not able to distinguish between the accreted and the '*in situ*' population (Di Matteo et al. 2019). Detailed, high-precision chemical inventory of a stellar population can do the job, especially in the high-metallicity regime (see e.g. Nissen & Schuster 2010, 2011). The *Gaia* RVS will provide metallicities and a limited set of chemical abundances in the future *Gaia* releases, but the sample will be magnitude limited. Past (e.g. Gilmore et al. 2012, Gaia-UVES Survey), ongoing (e.g. Allende Prieto et al. 2008, APOGEE), and future spectroscopic surveys (e.g. Dalton et al. 2018; de Jong et al. 2019, WEAVE and 4MOST) provided/are providing/will provide the detailed chemical informations missing from *Gaia*.

In recent years, a deep interest in the near-infrared (NIR) ranges was evident. Several spectrographs have been built or are under construction to observe the NIR ranges. A non-exhaustive list includes:

(i) CRIRES (Kaeufl et al. 2004) operated at the UT1, Antu telescope of the VLT, from 2006 to 2014, observing four intervals of the order of 5 nm wide, contained in the range 955 nm $\leq$ 5248 nm. The upgrade CRIRES will soon be available at VLT, with a higher capability in wavelength range coverage.

(ii) APOGEE (Allende Prieto et al. 2008) is a multi-object spectrograph, covering a wavelength range in the *H* band (1510–1700 nm), observing at intermediate resolution ($R \approx 22\,500$).

(iii) Multi-Object Optical and Near-infrared Spectrograph (MOONS, Cirasuolo et al. 2014) that will provide high-resolution ($R = 19\,700$) *H*-band spectra for 1000 targets over a field of view of 20 arcmin diameter at each pointing, as well as lower resolution *I*-band and *J*-band spectra.

(iv) GIANO (Origlia et al. 2014) is an NIR) cross-dispersed Echelle spectrograph, operating at Telescopio Nazionale Galileo (TNG). It covers the wavelength range 950–2450 nm and operate at high-resolving power ($R \approx 50\,000$).

(v) SPiRou[1]is an NIR cross-dispersed Echelle spectrograph, operating at Canada–France–Hawaii Telescope.

★ E-mail: serkor@skyline.od.ua

[1]http://spirou.irap.omp.eu/

(vi) CARMENES (Quirrenbach et al. 2014) is a cross-dispersed Echelle spectrograph with two arms: visible and NIR.

(vii) IRTF (InfraRed Telescope Facility) 3 m telescope on Maunakea equipped with cross-dispersed Echelle spectrograph iShell (1.08–5.3 micron, $R = 80000$, Rayner et al. 2016).

APOGEE is providing the community with a large amount of spectra (its release 16 provides more than 280 000 stellar spectra, Ahumada et al. 2019) and detailed chemical investigation (see e.g. Weinberg et al. 2019) for a significant sample of elements. However, the devil is in the details, to compare chemical abundances of stars spanning large ranges in effective temperature, derived in different spectral ranges, like visible and IR, to provide conclusions on the chemical evolution of the Galaxy, one should try to be as careful as possible. The departure from Local Thermodynamic Equilibrium (LTE) can play a role in affecting in different ways stars with different stellar parameters.

This paper is methodological in nature, and investigates how departures from LTE affect the individual lines of some chemical elements (Na, Mg, Al, S, K, and Sr) in the IR wavelength domain. For this purpose, we use the high-quality spectra of 40 dwarfs obtained with the GIANO spectrograph, already analysed by Caffau et al. (2019a) to derive stellar parameters and chemical compositions by using standard LTE approximation. Nevertheless, Caffau et al. (2019a) have also made the first attempt to evaluate the role of NLTE effects on the derived abundances, at least for a few elements (Na, Mg, Al, K, and Ca). We decided to revisit the abundances of those program stars and in this study we investigate the NLTE effects on the individual lines. We hope that our NLTE results will help other specialists to have the chance to provide careful abundance in their analysis based on IR spectra while using LTE approximation instead of NLTE analysis. We provide informations on which lines can be suitable for classic LTE analysis, producing quite reliable abundance results. To check the limits of applicability of our conclusions about the possibility of using the LTE approximation to derive the elemental abundances, we carried out an additional study of the problem by NLTE analysis for the more expanded field of atmospheric parameters. Qualitative results are presented in the Discussion section for each of the elements studied.

At our knowledge, no systematic investigation on NLTE has been done in the GIANO IR spectral domain. We here present results of our investigations. Among our sample of stars observed with GIANO there are 12 stars for which optical archive spectra are available (from various spectrographs, UVES, ESPaDOnS, Narval, and Sophie). All these spectra were also used for comparison of the abundances derived from the IR and optical spectra.

2 METHOD OF NLTE ANALYSIS AND INDIVIDUAL IONS

We first checked our NLTE atomic models to verify how adequately they reproduce the profiles of the IR lines of interest in the solar spectrum. The primary aim was to check the accuracy of oscillator strengths and damping parameters that are needed for calculations. We adopted the solar abundances derived in previous investigations from optical lines (see Table 1). We then investigated each line analysed in this work in the solar spectrum by comparing solar observations to the NLTE synthesis with the solar abundance derived from optical spectra and adopted here. The best choice would have been to use for this aim the solar spectrum observed with GIANO. Unfortunately, we had not such a spectrum in our disposal therefore we used solar atlases of Kurucz et al. (1984) (region < 12 500 Å), Reiners et al. (2016) (region 12 500–22 500 Å), ACE-FTS Hase et al. (2010) (region > 22 600 Å), and NSO/Kitt Peak FTS Livingston & Wallace (1991) (region 12 500–22 500 Å). We then adjusted the atomic data of each IR line here studied in a way to have a good agreement between the NLTE synthesis and the observed solar spectrum.

Table 1. Solar abundances adopted here.

Element	A(X)
Na	6.25
Mg	7.54
Al	6.43
S	7.16
K	5.11
Sr	2.92
Fe	7.52

In order to find atomic level populations for the following ions: Na I, Mg I, Al I, S I, K I, and Sr II, we employed the code MULTI (Carlsson 1986). For our aim, this program was modified and adapted by Korotin, Andrievsky & Luck (1999). MULTI enables one to calculate a single line NLTE profile. Nevertheless, the lines of interest are often blended in the real stellar spectra. In order to take the blending into account, we first calculate with MULTI the departure coefficients for those levels that form the line of interest, and then we include these coefficients in the LTE synthetic spectrum code SYNTHV (Tsymbal 1996). This allows one to calculate the source function and opacity for each studied line. Simultaneously, the blending lines are calculated in LTE with the help of line list and corresponding atomic data from VALD data base (Ryabchikova et al. 2015) in the wavelength range of the line under study.

For all our computations we have used 1D LTE atmosphere models computed with ATLAS9 code by Kurucz (1993, 2005). For our program stars, we used atmosphere parameters derived by Caffau et al. (2019a) with microturbulence velocity of 1 km s^{-1}. The atmospheric parameters $T_{\rm eff}$, log g, and [Fe/H] are presented in Table 2, where we adopted for the Sun A(Fe) = 7.52 (Caffau et al. 2011). The 12 stars, for which the NLTE abundances were also determined with the help of optical spectra, are marked in Table 2 with asterisks. The lines and atomic data used in the optical investigation of Na, Mg, Al, S, K, and Sr for these 12 stars were described in each introductive papers devoted to the NLTE atomic model for each ion. In Fig. 1, the sample of stars is presented in the $T_{\rm eff}$, log g plane; the 12 stars above mentioned are highlighted with blue crosses.

In the following sections, we shall compare our abundances both with those of Caffau et al. (2019a) for the same set of stars and with the abundances of a set of 41 552 stars with stellar parameters similar to our sample extracted from the APOGEE catalogue, SDSS data release 16 (Ahumada et al. 2019). The summary plots of this latter comparison are shown in Fig. 2.

To estimate the difference in the results between the NLTE and LTE approximations, for four representative stars of our sample, we determined the LTE abundances of the studied elements using the same set of lines and the same atomic parameters. The results are given in Table 3, where the LTE [X/Fe] is reported as well as the difference NLTE–LTE abundance (ΔNLTE in the Table). The choice of the four stars was driven by the desire to span the stellar parameter space. In Fig. 1, the selected stars are highlighted (red open circle) over the complete sample in the $T_{\rm eff}$, log g space.

Table 2. Atmosphere parameters of program stars and our NLTE abundances of the elements analysed.

Star	$T_{\rm eff}$ (K)	log g	[Fe/H]	[Na/Fe]	[Mg/Fe]	[Al/Fe]	[S/Fe]	[K/Fe]	[Sr/Fe]
HD 20670	5688	3.65	0.10	0.17 ± 0.10	0.11 ± 0.05	0.11 ± 0.07	0.02 ± 0.06	0.05 ± 0.12	− 0.03 ± 0.03
HD 24040*	5809	4.12	0.09	0.09 ± 0.12	0.08 ± 0.05	0.10 ± 0.10	− 0.04 ± 0.08	− 0.01 ± 0.12	− 0.05 ± 0.02
HD 28005*	5802	4.18	0.21	0.21 ± 0.10	0.05 ± 0.07	0.10 ± 0.10	0.00 ± 0.07	0.02 ± 0.12	− 0.08 ± 0.03
HD 32673	5752	3.53	0.07	0.13 ± 0.10	0.16 ± 0.05	0.17 ± 0.07	− 0.01 ± 0.07	0.03 ± 0.10	0.01 ± 0.04
HD 34445*	5803	4.06	−0.03	0.13 ± 0.10	0.11 ± 0.05	0.11 ± 0.10	0.07 ± 0.07	0.04 ± 0.10	0.06 ± 0.03
HD 34575*	5582	4.22	0.18	0.07 ± 0.10	0.10 ± 0.06	0.07 ± 0.08	− 0.06 ± 0.08	0.01 ± 0.12	− 0.05 ± 0.05
HD 44420	5777	4.23	0.19	0.15 ± 0.13	0.02 ± 0.05	0.18 ± 0.12	0.02 ± 0.10	0.02 ± 0.12	0.00 ± 0.03
HD 56303	5941	4.21	0.05	0.02 ± 0.10	0.07 ± 0.06	0.07 ± 0.08	− 0.02 ± 0.08	− 0.01 ± 0.10	0.08 ± 0.04
HD 67346	5953	3.78	0.14	0.11 ± 0.15	0.07 ± 0.06	0.07 ± 0.10	0.03 ± 0.10	− 0.02 ± 0.10	0.07 ± 0.04
HD 69056	5637	4.28	0.05	0.01 ± 0.10	0.10 ± 0.05	0.15 ± 0.10	− 0.01 ± 0.10	0.04 ± 0.10	0.00 ± 0.05
HD 69809	5842	4.16	0.17	0.13 ± 0.12	0.08 ± 0.06	0.12 ± 0.08	0.01 ± 0.08	− 0.03 ± 0.10	− 0.06 ± 0.03
HD 69960	5655	3.99	0.22	0.08 ± 0.10	0.02 ± 0.06	0.08 ± 0.10	− 0.02 ± 0.08	− 0.01 ± 0.10	− 0.08 ± 0.05
HD 73226	5886	4.21	0.06	0.04 ± 0.12	0.03 ± 0.06	0.06 ± 0.10	− 0.02 ± 0.07	0.01 ± 0.08	0.03 ± 0.01
HD 73933	6143	4.24	0.06	− 0.08 ± 0.12	0.04 ± 0.05	0.02 ± 0.10	− 0.03 ± 0.08	− 0.01 ± 0.10	0.14 ± 0.06
HD 76909	5655	4.17	0.24	0.14 ± 0.15	0.07 ± 0.07	0.07 ± 0.08	0.02 ± 0.10	0.01 ± 0.10	0.00 ± 0.07
HD 77519	6140	3.85	0.14	0.01 ± 0.12	0.08 ± 0.06	0.09 ± 0.15	0.03 ± 0.12	− 0.01 ± 0.10	0.14 ± 0.05
HD 82943*	5917	4.23	0.13	0.10 ± 0.12	0.03 ± 0.06	0.06 ± 0.10	0.00 ± 0.07	− 0.07 ± 0.10	0.01 ± 0.04
HD 85301	5640	4.44	0.05	-0.05 ± 0.12	− 0.03 ± 0.04	− 0.04 ± 0.10	0.02 ± 0.12	0.01 ± 0.08	0.19 ± 0.04
HD 87359*	5645	4.40	−0.07	0.01 ± 0.10	0.10 ± 0.06	0.04 ± 0.10	0.08 ± 0.07	0.01 ± 0.12	0.09 ± 0.06
HD 87836	5684	4.05	0.16	0.22 ± 0.12	0.09 ± 0.05	0.13 ± 0.10	0.02 ± 0.10	0.01 ± 0.10	0.03 ± 0.05
HD 90681	5950	4.26	0.16	− 0.02 ± 0.12	0.04 ± 0.06	0.05 ± 0.07	− 0.04 ± 0.12	− 0.04 ± 0.10	− 0.02 ± 0.05
HD 90722	5677	4.12	0.22	0.08 ± 0.12	0.04 ± 0.05	0.09 ± 0.10	− 0.04 ± 0.10	− 0.02 ± 0.10	− 0.05 ± 0.03
HD 92788*	5694	4.26	0.13	0.15 ± 0.15	0.07 ± 0.10	0.15 ± 0.10	0.06 ± 0.07	− 0.04 ± 0.15	0.04 ± 0.05
HD 97645	6127	4.10	0.14	− 0.02 ± 0.15	0.02 ± 0.04	0.09 ± 0.10	− 0.02 ± 0.12	− 0.02 ± 0.12	0.06 ± 0.05
HD 98618*	5727	4.27	−0.11	0.07 ± 0.08	0.08 ± 0.06	0.08 ± 0.07	0.11 ± 0.08	0.00 ± 0.12	0.13 ± 0.04
HD 98736*	5276	4.40	0.29	0.17 ± 0.15	− 0.03 ± 0.07	0.06 ± 0.10	− 0.04 ± 0.10	− 0.08 ± 0.15	− 0.11 ± 0.08
HD 99491	5537	4.40	0.25	0.15 ± 0.12	0.04 ± 0.07	0.14 ± 0.10	− 0.07 ± 0.12	0.03 ± 0.12	− 0.06 ± 0.06
HD 99492*	5006	4.56	0.20	0.22 ± 0.12	0.00 ± 0.09	0.17 ± 0.15	− 0.05 ± 0.12	− 0.03 ± 0.15	− 0.03 ± 0.06
HD100069	5796	3.74	−0.03	0.08 ± 0.15	0.11 ± 0.08	0.13 ± 0.10	0.06 ± 0.08	0.06 ± 0.12	0.09 ± 0.04
HD105631	5391	4.47	0.05	− 0.01 ± 0.12	0.04 ± 0.06	0.03 ± 0.08	0.03 ± 0.08	0.02 ± 0.10	0.10 ± 0.04
HD106116	5665	4.30	0.03	0.10 ± 0.10	0.05 ± 0.06	0.11 ± 0.08	0.00 ± 0.08	0.04 ± 0.10	0.05 ± 0.03
HD106156	5449	4.45	0.10	0.04 ± 0.12	0.04 ± 0.08	0.05 ± 0.15	0.02 ± 0.12	0.01 ± 0.08	0.01 ± 0.04
HD108942	5882	4.27	0.20	0.08 ± 0.15	0.00 ± 0.08	0.04 ± 0.10	− 0.09 ± 0.10	0.02 ± 0.10	− 0.05 ± 0.06
HD114174	5728	4.30	−0.06	0.09 ± 0.10	0.08 ± 0.07	0.11 ± 0.10	0.02 ± 0.10	0.07 ± 0.10	0.28 ± 0.06
HD116321	6292	3.66	0.10	0.18 ± 0.20	0.13 ± 0.04	0.20 ± 0.18	0.06 ± 0.12	− 0.01 ± 0.12	0.17 ± 0.08
HD136618	5805	3.56	0.14	0.18 ± 0.18	0.09 ± 0.05	0.10 ± 0.12	− 0.03 ± 0.10	− 0.02 ± 0.10	0.02 ± 0.05
HD145675*	5312	4.37	0.33	0.18 ± 0.15	0.06 ± 0.04	0.07 ± 0.10	− 0.02 ± 0.09	− 0.03 ± 0.10	− 0.11 ± 0.06
HD147231	5594	4.30	−0.14	0.09 ± 0.15	0.22 ± 0.09	0.09 ± 0.15	0.07 ± 0.10	0.20 ± 0.12	0.05 ± 0.06
HD159222	5815	4.30	0.00	0.05 ± 0.10	0.05 ± 0.03	0.05 ± 0.10	0.04 ± 0.10	− 0.04 ± 0.12	0.08 ± 0.06
HD190360*	5424	4.21	−0.01	0.11 ± 0.12	0.17 ± 0.08	0.18 ± 0.10	0.20 ± 0.09	0.08 ± 0.12	0.05 ± 0.05

2.1 Na I

The NLTE sodium model atom was first described in Korotin & Mishenina (1999) and later updated by Dobrovolskas et al. (2014). This model provides the NLTE solar sodium abundance A(Na) = 6.25, derived from optical lines and reported in Table 1. The oscillator strengths for the 1074.6–1267.9 nm lines were taken from Wiese, Smith & Miles (1969), for the 2205.6 and 2208.3 nm lines from McEachran & Cohen (1983), and for the 2334.8–2337.9 nm lines from the NIST data base (Reader, Kramida & Ralchenko 2012).

The theoretical NLTE synthesis of the 996.1 nm line cannot reproduce the observed solar spectrum, as well as the 2145.2 nm line. The problem is that these observed lines are weaker than in the theoretical synthesis. The estimated NLTE effects cannot explain such a difference, therefore those lines were excluded from the analysis.

For all the lines (except one at 1267.9 nm), we took van der Waals parameter: $\Gamma_{\rm vw} = -7.06$ (hereafter we use $\Gamma_{\rm vw}$ as a log of the line full width at half-maximum per perturber at $T = 10\,000$ K in cgs units). This value is slightly larger than the estimated value from Unsöld's formula (Unsöld 1955) but it provides a better fit with observed solar profile.

For the atomic model of sodium, as well as for the other models considered here, we must make the following remark. Correction of $\Gamma_{\rm vw}$, if necessary, is performed only for lines with developed wings. For such lines, the influence from the accepted value of $\Gamma_{\rm vw}$ is higher than from the uncertainty of the oscillator strength (the latter possibility, of course, is not excluded). Such line profiles cannot be adjusted only by changing the element abundance or the value of log gf.

Below we list some notes on individual lines when comparing the NLTE theoretical synthesis to the observed solar spectrum.

(i) The synthesis of the line at 1074.644 nm reproduces very well the observed solar spectrum.

(ii) The lines at 1083.484, 1083.484, and 1083.490 nm give abundances by about 0.1 dex lower than our adopted solar sodium abundance.

(iii) The lines at 1267.917, 1267.917, and 1267.922 nm give abundances by 0.05 dex higher than our NLTE solar sodium

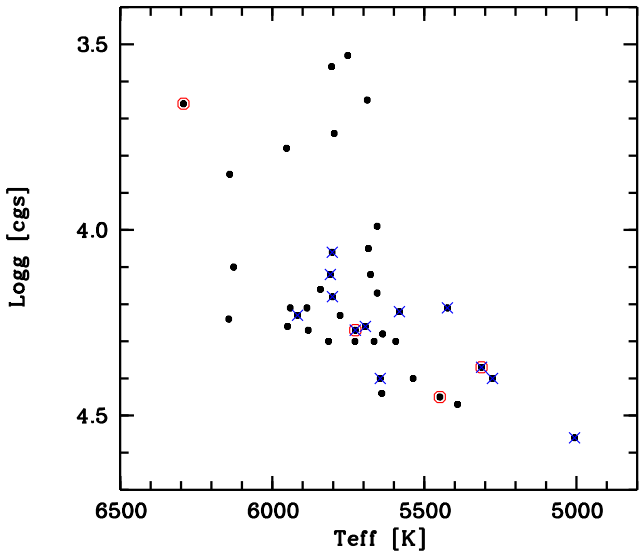

Figure 1. The stellar parameters of the complete sample (filled black circles). The four stars for which the LTE–NLTE comparison has been made have a red circle around the black symbol. The 12 stars for which we performed an optical investigation are highlighted with a blue cross.

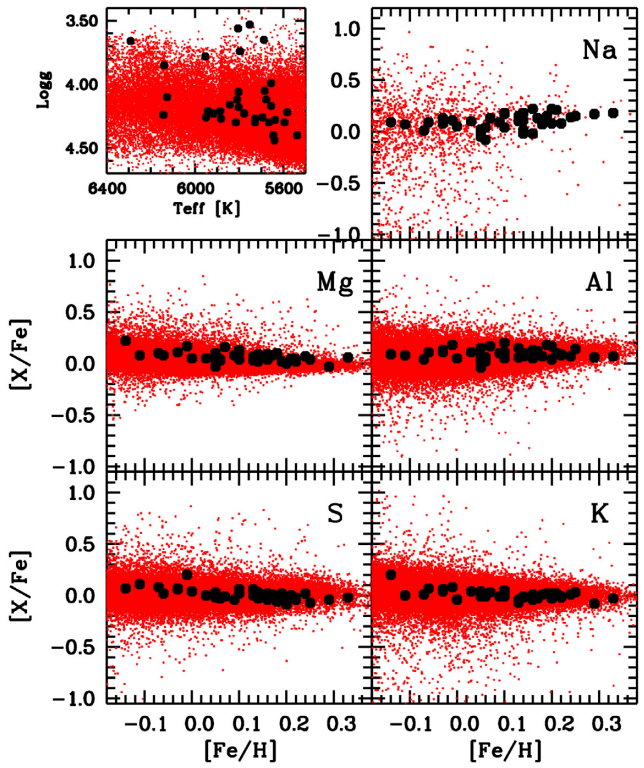

Figure 2. The parameters and abundances of the stars here analysed (black filled circles) compared to the APOGEE DR16 data.

abundance. Γ_{vw} for these lines was taken from Barklem, Piskunov & O'Mara (2000).

(iv) For three lines (2205.640, 2208.366, and 2334.837 nm), the agreement between the NLTE theoretical synthesis and the solar observed spectrum is very good, while in the two lines at 2337.896 and 2337.914 nm a higher solar abundance (by 0.04 dex) would be needed to reproduce the solar observed spectrum.

(v) All the lines are formed practically in LTE (equivalent widths (EW) vary in the range from –2 per cent to +4 per cent).

(vi) The exception is multiplet 2334.8–2337.9 nm whose lines in NLTE are strengthened by about 7–15 per cent.

It is possible that a deviation within 0.1 dex of the sodium content obtained from the individual lines listed above from the adopted solar sodium abundance of Table 1 may be due to inaccuracy of our adopted oscillator strengths. An investigation of this issue is beyond the scope of this work. Similar conclusion can also be applied to some lines of other ions, discussed below.

Our NLTE abundance of sodium in the program stars differ from LTE abundances obtained by Caffau et al. (2019a) from 0 to 0.25 dex. On average, our NLTE abundance is 0.09 dex higher than the LTE abundance of Caffau et al. (2019a). We should stress that this comparison is not just as NLTE−LTE difference because the lines used are not the same and the atomic parameters used neither.

The relative abundance [Na/Fe] of our sample stars shows a weak trend with metallicity, the effect is an increase with increasing metallicity (the range is from –0.08 to 0.22 dex). A non-parametric test with Kendall's τ provides in fact a correlation probability of 99 per cent. The same test on the subset of 1679 stars with Na measurements shows also a 99 per cent probability of correlation. If we divide the two samples in 0.1 dex metallicity bins, the GIANO sample has σ in each bin that ranges from 0.007 to 0.080 dex. For the APOGEE sample it ranges from 0.27 to 0.36 dex. The mean abundance for the 40 stars is [Na/Fe] = +0.09 ± 0.07. It should be noted that the abundance from IR lines agrees well with abundance derived from optical lines (the mean deviation is only +0.03 dex). Individual deviations do not exceed ±0.06 dex.

In Appendix (Fig. A1), we show some examples of the observed and synthetic NLTE and LTE profiles of two sodium lines in the solar and stellar observed spectra. Fig. 3 shows the derived NLTE sodium abundances for our sample of stars versus [Fe/H] and [Mg/H] (α-element). The A(Fe) determination is from Caffau et al. (2019a), so it is in LTE while the A(Mg) is the value here derived in NLTE. We understand the inconsistency in mixing LTE and NLTE abundances, but still we think useful to provide, for each element, [X/Fe] versus [Fe/H], which is what usually presented in the literature.

The NLTE effects for Na in this stellar parameter space are well within the uncertainties, being for the four representative stars at maximum –0.04 dex.

2.2 Mg I

The NLTE magnesium (Mg I) atomic model was described in Mishenina et al. (2004) and later updated by Černiauskas et al. (2017). Our NLTE solar magnesium abundance from optical lines is A(Mg) = 7.54 (see Table 1). The oscillator strength for the 1081.12 nm line was taken from Kurucz & Peytremann (1975); for the 1203.9–1208.3 nm lines – from Chang & Tang (1990), and for other lines – from NIST data base (the latter uses mainly the results of calculations by Butler, Mendoza & Zeippen 1993). The van der Waals parameters were calculated using Unsöld's formula and then corrected with the help of lines from solar spectrum. For line at 1182.8 nm, we used the value reported in Barklem et al. (2000). NLTE effects lead to the strengthening of the line in vicinity of the core, while the wings remain practically unchanged. The lines at 982.1, 982.8, 998.3, and 998.6 nm are formed practically in LTE. To fit the synthetic line profiles to the solar observed ones, by keeping our adopted solar abundance, one needs to increase the oscillator

Table 3. LTE abundances for selected stars.

Star	$T_{\rm eff}$ (K)	log g	[Fe/H]	[Na/Fe]	$\sigma_{\rm LTE}$	ΔNLTE	[Mg/Fe]	$\sigma_{\rm LTE}$	ΔNLTE	[Al/Fe]	$\sigma_{\rm LTE}$	ΔNLTE
HD98618	5727	4.27	−0.11	0.09 ± 0.09	0.04	−0.02	0.12 ± 0.07	0.04	−0.04	0.13 ± 0.09	0.06	−0.05
HD106156	5449	4.45	0.10	0.06 ± 0.14	0.07	−0.02	0.08 ± 0.10	0.06	−0.04	0.12 ± 0.16	0.06	−0.07
HD116321	6292	3.66	0.10	0.22 ± 0.25	0.15	−0.04	0.15 ± 0.06	0.04	−0.02	0.26 ± 0.19	0.04	−0.06
HD145675	5312	4.37	0.33	0.21 ± 0.16	0.04	−0.03	0.10 ± 0.06	0.05	−0.04	0.12 ± 0.11	0.03	−0.05
Star	$T_{\rm eff}$, K	log g	[Fe/H]	[S/Fe]	$\sigma_{\rm LTE}$	ΔNLTE	[K/Fe]	$\sigma_{\rm LTE}$	ΔNLTE	[Sr/Fe]	$\sigma_{\rm LTE}$	ΔNLTE
HD98618	5727	4.27	−0.11	0.14 ± 0.11	0.07	−0.03	0.18 ± 0.15	0.09	−0.18	0.41 ± 0.05	0.03	−0.28
HD106156	5449	4.45	0.10	0.04 ± 0.14	0.04	−0.02	0.18 ± 0.14	0.12	−0.17	0.25 ± 0.05	0.03	−0.24
HD116321	6292	3.66	0.10	0.14 ± 0.18	0.13	−0.08	0.20 ± 0.18	0.13	−0.21	0.62 ± 0.09	0.03	−0.45
HD145675	5312	4.37	0.33	0.00 ± 0.10	0.04	−0.02	0.11 ± 0.14	0.10	−0.14	0.07 ± 0.07	0.04	−0.18

Note. $\sigma_{\rm LTE}$ – the additional error introduced by the use of LTE approximation.

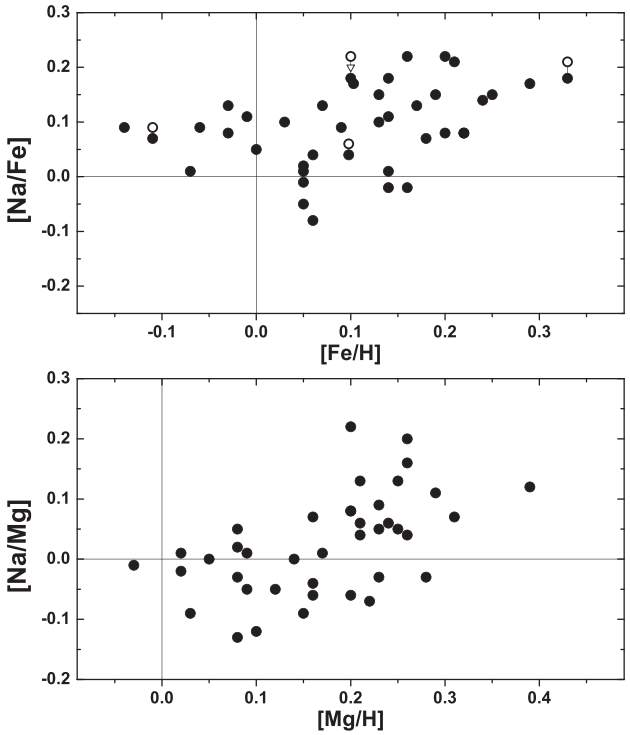

Figure 3. Relative sodium abundances ([Na/Fe] and [Na/Mg]) as a function of [Fe/H] (*upper panel*) and [Mg/H] (*lower panel*). The NLTE abundances are indicated by *filled circles*. For comparison, we show also the LTE sodium abundances for the four selected stars (*open circles*). The arrow lines connect the LTE and NLTE abundance values for the same stars. The numerical values of LTE abundances are listed in Table 3.

strengths of these lines by about 0.08 dex, which is of the same order of magnitude of the line-to-line scatter for the Mg investigation (see Table 2).

Some comments on the lines here below about the solar study of the Mg lines.

(i) The feature at 1081.1 nm is formed by eight components. The NLTE corrections are not negligible (exceed 5 per cent in EW). The wings of this feature can be adjusted if $\Gamma_{\rm vw}$ is decreased from −6.68 (Barklem et al. 2000) to −6.82 (the value derived from the solar spectrum).

(ii) The lines at 1095.3, 1095.7, and 1096.5 nm are formed practically in LTE.

(iii) For line at 1182.8 nm, the NLTE correction in EW achieves 6 per cent.

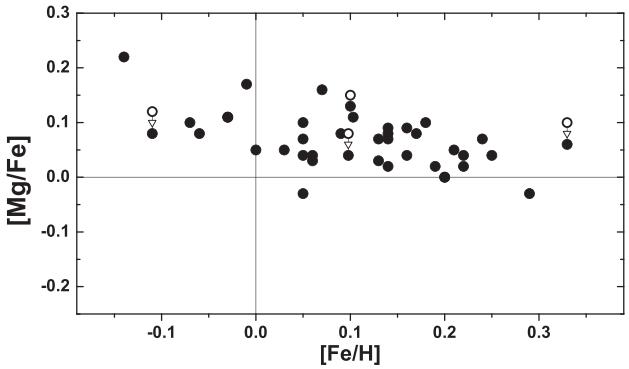

Figure 4. Same as Fig. 3 (upper panel) but for magnesium.

(iv) The line at 1203.9 nm is formed practically in LTE.

(v) The NLTE effect for the 1208.3 nm feature is modest (about 5 per cent in EW). This feature is a blend of two lines. The wing of this blend can be adjusted if $\Gamma_{\rm vw}$ is decreased from −6.98 (Barklem et al. 2000) to −7.12 (from the solar spectrum).

(vi) The lines at 1241.7, 1242.3, and 1243.3 nm are formed practically in LTE.

(vii) The lines at 1502.4, 1504.0, and 1504.7 nm show very small NLTE effects.

(viii) The lines at 1574.0, 1574.8, and 1576.5 nm also show very small NLTE effects.

(ix) For the 1710.8 nm line, the NLTE effects are about 5 per cent in EW.

The NLTE correction for Mg for the four selected stars is small, up to −0.04 dex. In Appendix (Fig. A1), we show NLTE and LTE profiles of two magnesium lines in the solar and stellar spectra. Fig. 4 is the same as Fig. 3 but for magnesium.

From our data, one can infer a decrease of the [Mg/Fe] ratio with increasing metallicity with a probability of over 99 per cent. Such a decrease is also clear from the APOGEE data, however the decrease is not as steep as in our data. Our [Mg/Fe] ratios are higher than the APOGEE data by about 0.08 dex for the lowest metallicity bin and converge towards the APOGEE values at higher metallicities.

2.3 Al I

The aluminium NLTE atomic model is described in detail in Andrievsky et al. (2008) and Caffau et al. (2019b). Our adopted NLTE solar abundance is A(Al) = 6.43 (see Table 1). The van der Waals parameters for the IR lines were obtained from Unsöld's formula. For some lines, the van der Waals parameters were

corrected using the solar spectrum. Some details on individual lines while comparing theoretical NLTE profile to the observed solar spectrum are given below.

(i) The line at 1087.297 nm (NIST log gf) is very well modelled by the synthetic spectrum. This line is formed in LTE.

(ii) The line at 1089.174 nm (NIST log gf) cannot be reproduced by theoretical synthesis. Probably this line is a blend, because its log gf listed in NIST has an accuracy better than 10 per cent. The estimated NLTE correction is negligible for this line.

(iii) The theoretical NLTE profile of line at 1312.341 nm (log gf are from Wiese et al. 1969) reproduces very well the observed solar profile, once the Γ_{vw} is adjusted. The LTE profile is wider in the wings but shallower in the core compared to observed profile. The NLTE EW in the solar spectrum appears to be somewhat larger but not very significantly (3–5 per cent) with respect to the LTE EW. For the stars, this difference can be larger (up to 13 per cent, which corresponds to 0.15 dex in abundance).

(iv) The line at 1315.075 nm (log gf are from Wiese et al. 1969 and Γ_{vw} was derived to fit the solar spectrum) is blended in the solar spectrum with a telluric line. However, the profile of this line in the spectra of the studied stars is well described with the same abundance as derived from the 1312.3 nm line. The value of the Γ_{vw} is taken the same as for the line 1312.3 nm of the same multiplet. Therefore, we can assume that parameters of this line are fairly reliable.

(v) Synthetic profile of the line at 1671.896 nm (NIST log gf and Γ_{vw} were optimized to reproduce the solar spectrum) is weaker than the observed one. This result cannot be attributed to an inaccuracy in log gf value, since the accuracy on the oscillator strength is better than 3 per cent. The core of the line profile in LTE is shallower than what is calculated in NLTE. In any case NLTE effects are small for this line.

(vi) The central part of the line at 1675.056 nm (NIST log gf and Γ_{vw} were adjusted to fit the solar spectrum) is blended with a telluric line in the solar spectrum. This does not allow us to estimate the accuracy of the value log gf. In the stellar spectra, the synthetic profile of this line is systematically weaker than observed one. The difference is not the result of the log gf inaccuracy, since it is better than 3 per cent.

(vii) The line at 1676.336 nm (NIST log gf and Γ_{vw} were adjusted to fit the solar spectrum) is described very well in the solar spectrum. For the stellar spectra, the difference LTE and NLTE in EW can achieve up to 4 per cent (which corresponds to 0.05 dex in abundance).

(viii) The line at 2109.303 nm (log gf is from Kurucz & Peytremann 1975) does not allow us to check the value of Γ_{vw}. Therefore, we use the parameter Γ_{vw} the same as for the line 2116.376 nm of the same multiplet. For the stars, the abundance derived from this line, agrees with abundance derived from the line at 2116.3 nm. LTE profile of this line is shallower than in the observed spectrum. For the Sun, the NLTE EW is slightly larger but insignificant (3–5 per cent) than the LTE value. For the stellar spectra, this difference can achieve up to 12 per cent.

(ix) The NLTE synthetic profile of the line at 2116.376 nm (log gf is from Kurucz & Peytremann 1975 and Γ_{vw} was derived from the solar spectrum) reproduces very well the solar observed spectrum.

In order to derive aluminium abundance in the dwarf stars, using GIANO spectra, we used the following lines: 1087.2, 1312.3, 1315.0, 1671.8, 1676.3, 2109.3, and 2116.3 nm. The abundance of aluminium derived from the IR lines is practically the same as

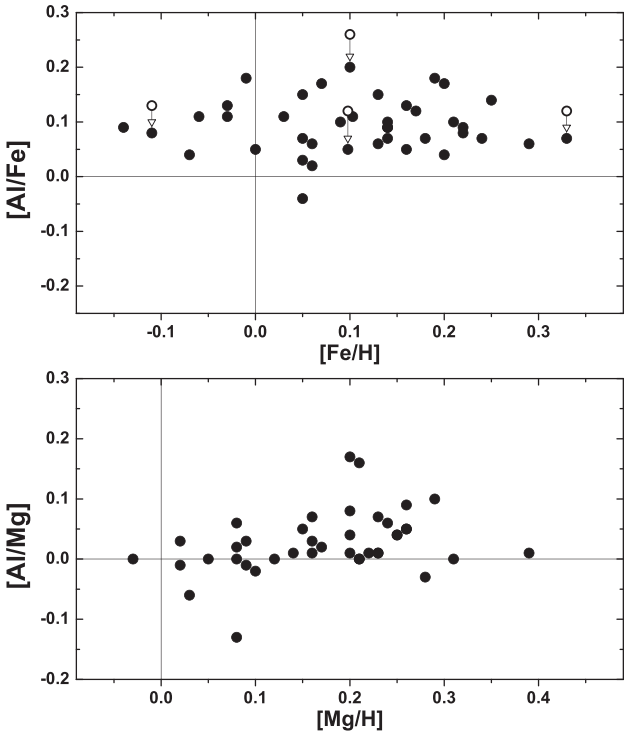

Figure 5. Same as Fig. 3 but for aluminium.

from the optical lines at 669.6, 669.8, 736.1, 736.2, 783.5, 783.6, 877.2, and 877.3 nm. The difference is no more than 0.04 dex. Our NLTE aluminium abundance differs from LTE abundance derived by Caffau et al. (2019a) up to ±0.15 dex. The mean difference is about 0.05 dex (our value is lower) but this difference is probably due to the differences in adopted atomic data and lines used.

[Al/Fe] does not show any dependence on metallicity. This value is distributed in the range from −0.05 to 0.20 dex with a mean value from 40 stars [Al/Fe] = +0.09 ± 0.05.

The NLTE correction we derived for the four selected stars is small, on average about −0.06 dex. In Appendix (Fig. A1), we show NLTE and LTE profiles of two aluminium lines in the solar and stellar spectra. Fig. 5 is the same as Fig. 3 but for aluminium.

2.4 S I

The sulphur NLTE model is described in detail in Korotin (2009). For the solar sulphur abundance this model, used in the optical wavelength range, provides A(S) = 7.16 (see Table 1). For the lines at 921.2–923.7 nm, the oscillator strengths we applied are from Biemont, Quinet & Zeippen (1993), as well as for the lines at 2250.0–2270.0 nm. The synthetic profiles of the lines at 1045.5, 1045.6, and 1045.9 nm are in good agreement with the solar spectrum when using values log gf from Wiese et al. (1969). Van der Waals parameters for these lines are from Barklem et al. (2000).

For the lines in the region 1540.0–1542.3 nm, the oscillator strengths were taken from two sources: Biemont et al. (1993) and NIST. It should be noted that the log gf from NIST are lower by 0.18 dex with respect to the data of Biemont et al. (1993). The same is valid for the lines of the multiplet at 1546.9–1547.9 nm, where the difference between the log gf is 0.16 dex. The lines at 1540.0 and 1540.3 nm are blended with telluric lines in the solar spectrum, therefore we cannot use them to check their parameters. The lines

at 1542.3, 1546.9, 1547.5, and 1547.8 nm are clean, and we found that their log gf values can be decreased by 0.1 dex (with respect to the data of Biemont et al. 1993) to achieve a good agreement with the observed profiles in the solar spectrum. It is important to note that these lines are weak in the solar spectrum (residual intensity is larger than 0.85) therefore the influence of the accepted values of log gf on their calculated strength is predominant. Thus, we one can conclude that, most likely, the real values of log gf for mentioned lines appear to be between the data of Biemont et al. (1993) and NIST. The NIST accuracy for these oscillator strengths are ≥25 per cent, and they are listed in Table A1. The lines at 2250.7 and 2251.9 nm are reproduced with a reasonable agreement in the solar spectrum but the continuum in this region is not quite reliable. The lines at 2255.2, 2256.3, 2257.5, and 2264.4 nm are slightly blended with telluric lines in the solar spectrum, and the line at 2270.7 nm is very well reproduced by a synthetic profile.

Actually, in our NLTE analysis of dwarf spectra we used the following lines: 1045.5, 1045.6, and 1045.9 nm (principal lines for which NLTE corrections are moderate: EWs are up to 25 per cent, i.e. −0.3 dex in abundance). The NLTE corrections increase as effective temperature increases. For most stars, the corrections are within 0.15 dex. The lines at 1540.0–1547.9 nm have the NLTE corrections up to 5 per cent in EW. For these lines, we derive a correction in abundance of +0.10 dex, which can be due to an inaccuracy of the oscillator strengths (see discussion in the beginning of this subsection). The lines at 2250.7, 2251.9, 2255.2, 2257.5, 2256.3, 2264.4, and 2270.7 nm are formed almost in LTE (difference in EWs is about 3 per cent).

For our analysis in the optical range, we used the following lines: 921.2, 922.8, and 923.7 nm (large NLTE corrections: from −0.13 to −0.18 dex), 869.3 and 869.4 nm (corrections are rather small: from −0.05 to −0.03 dex), 674.3, 674.8, 675.7, and 605.2 nm (lines are formed almost in LTE). The agreement between the abundances derived from GIANO spectra and the UVES and ESPaDOnS spectra is excellent (within the range of 0.04 dex). Our NLTE sulphur abundances for individual stars differ from LTE values of Caffau et al. (2019a) from −0.17 to 0.15 dex and our mean NLTE abundance for all sample of stars is about 0.02 dex lower than the mean LTE value derived by Caffau et al. (2019a), but these comparisons are related to the difference in selected atomic data and lines used, not to NLTE effects. The ratio [S/Fe] demonstrates a prominent increase with metallicity decrease (probability over 99 per cent). Such an increase is statiscally apparent also in the APOGEE data, however in our data it is considerably steeper, with [S/Fe] ratios higher than in the APOGEE data at the lowest metallicities and lower at the highest metallicity, with a cross-over at about 0.1 dex. The ratios for individual stars are within the interval from −0.09 to 0.20 dex. The mean value from 40 stars is [S/Fe] = +0.01 ± 0.05.

The sulphur NLTE correction, we derived for the four selected stars, is negligible for the three cooler stars, for the hottest star it is −0.08 dex, but anyway smaller than the line-to-line scatter. In Appendix (Fig. A1), we show NLTE and LTE profiles of two sulphur lines in the solar and stellar spectra. Fig. 6 is the same as Fig. 3 but for sulphur.

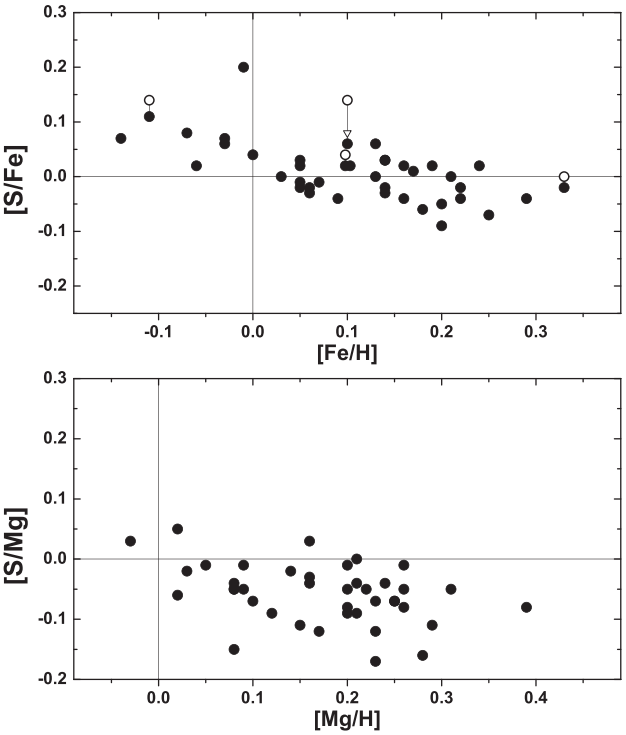

Figure 6. Same as Fig. 3 but for sulphur.

2.5 K I

The potassium NLTE atomic model was described in Andrievsky et al. (2010). The basic atomic model was modified: photoionization cross-sections for some levels were added following to the data from by Zatsarinny & Tayal (2010); then, for the six lower levels collisional rates with hydrogen atoms were added (Belyaev & Yakovleva 2017). The oscillator strengths for the lines at 1176.9 and 1177.2 nm were taken from Safronova, Safronova & Clark (2013), for other lines – from Wiese et al. (1969). For the lines at 1176.9, 1177.2, 1243.2, and 1252.2 nm damping parameters Γ_{vw} are from Barklem et al. (2000). For the lines at 1516.3 and 1516.8 nm, van der Waals parameters were calculated with the help of from Unsöld's formula. Our solar potassium abundance derived from the optical range is A(K) = 5.11 (see Table 1). All potassium lines in the IR domain of the solar spectrum are strengthened due to NLTE effects (abundance corrections are from 0.03 to 0.18 dex).

There are some important details. In the stellar spectra, the right wing of the 1176.9 nm line is distorted by CN lines. In the solar spectrum these lines are separated, and potassium line is well reproduced by theoretical synthesis. A telluric absorption blends the 1177.2 nm line in the solar spectrum. The line at 1243.2 nm is well reproduced by the synthetic profile. The left wing of the 1252.2 nm line in the stellar spectra is distorted by the presence of the 1252.181 nm Cr I line, but it is not a problem for the solar spectrum. The line at 1516.3 nm is situated in a telluric absorption wing in the solar spectrum. In the stellar spectra, the left wing of this line is distorted by the presence of the 1516.265 nm CN band. This line is formed in LTE. Similar situation is seen for the 1516.8 nm line, which is also blended by a telluric line, and formed in LTE. The right wing of this line in the stellar spectra is distorted by the 1516.866 nm CN band and the 1516.887 nm Fe I line.

For the stellar spectra, we used as a rule the 1176.9, 1177.2, 1243.2, and 1252.2 nm lines. The lines at 1516.3 and 1516.8 nm were used as auxiliary lines (since they are partially blended with CN bands). In order to compare the abundances from GIANO to those derived from UVES and ESPaDOnS, we used the 766.4 and 769.8 nm lines. We found that the differences in abundances are within 0.05 dex. Only for one star, HD98736, the difference was

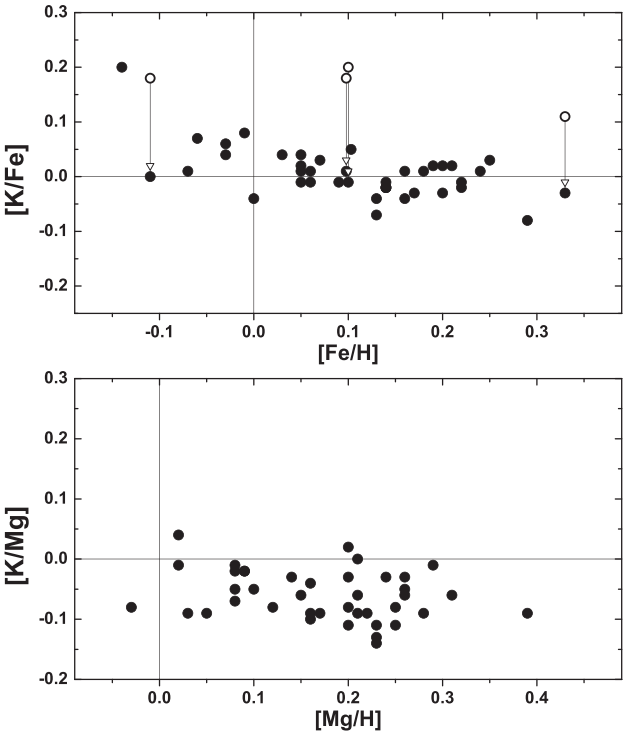

Figure 7. Same as Fig 3 but for potassium.

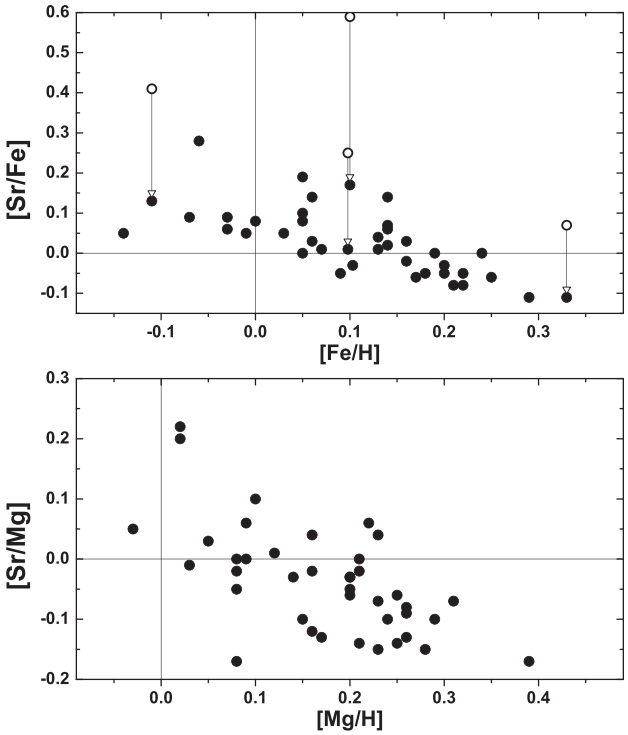

Figure 8. Same as Fig. 3 but for strontium.

0.11 dex (the abundance from IR lines is higher). The difference of the mean abundances from NLTE analysis and LTE analysis by Caffau et al. (2019a) is up to 0.3 dex; in this difference the NLTE effects play a part but the difference is also related to atomic data choice. [K/Fe] versus [Fe/H] shows a small increase of the potassium abundance as metallicity decreases, this is statistically significant (99.7 per cent). A similar increase is statistically apparent also in the APOGEE data, although impossible to detect visually, even after binning the data in metallicity. The mean potassium abundance based on the 40 stars is [K/Fe] $= +0.01 \pm 0.05$.

The NLTE correction, we derived for the four selected stars, is not negligible; it is comparable to or slightly larger than the uncertainty on the abundance determination. In Appendix (Fig. A1), we show NLTE and LTE profiles of two potassium lines in the solar and stellar spectra. Fig. 7 is the same as Fig. 3 but for potassium.

2.6 Sr II

The strontium NLTE atomic model is from Andrievsky et al. (2011). Our solar strontium abundance derived from the solar optical spectrum is A(Sr) = 2.92 (see Table 1). Synthetic spectra of the three lines at 1003.6, 1032.7, and 1091.4 nm (log gf are from Warner 1968 and Γ_{vw} are from Barklem et al. 2000) are able to well reproduce the solar observed spectrum. We found that NLTE effects strongly influence these lines. As a rule, the line EWs in the solar spectrum are increased by 20–25 per cent, but in some cases the NLTE corrections achieve about 0.20–0.36 dex. The mean NLTE abundance differs from the LTE abundance published by Caffau et al. (2019a) by about 0.5 dex. Surely, in this difference the NLTE plays a big role. The [Sr/Fe] ratio shows a clear dependence on [Fe/H]: the lower the metallicity, the larger the [Sr/Fe] ratio. When [Fe/H] $= +0.10$, [Sr/Fe] equals to zero.

The NLTE correction, we derived for the four selected stars, is in the range from -0.18 (for the coolest star) to -0.45 (for the hottest star). Being the uncertainty on the abundance determination small (always within 0.1 dex), for these Sr lines the NLTE effect should be taken into account, when possible. In Appendix (Fig. A1), we show NLTE and LTE profiles of two strontium lines in the solar and stellar spectra. Fig. 8 is the same as Fig. 3 but for strontium.

3 DISCUSSION

The main goal of this investigation was to provide, for Na I, Al I, Mg I, S I, K I, and Sr II, a list of lines in the IR wavelength range that can be safely used in an LTE investigation. The selected lines, covering the complete wavelength range of GIANO (950–2450 nm), are listed in Table A1. In the Table, we provide the oscillator strength, the Γ_{vw}, and a comment on the line: LTE means the line can safely be analysed in the LTE approximation (absolute NLTE correction is smaller than 0.02 dex), while NLTE means that the line is affected by departure from LTE. For a few lines, the string 'small NLTE' means that there is a minor NLTE effect (not larger than 5 per cent in EW). These computations can safely be applied for unevolved, solar metallicity stars, with stellar parameters similar to the sample here analysed (see Fig. 1). Clearly, in another parameter space NLTE effects can be different. In Fig. A1, for a few selected lines the observed profiles of the Sun and of the three stars (HD 20670, HD 24040, and HD 114174) are compared to the LTE and NLTE theoretical profiles. As one can see, the agreement of NLTE synthetic profile with the observed spectrum is very good, while for several cases the theoretical LTE profile deviates from the observation.

The trends of the investigated elements as a function of the metallicity confirm the ones that are apparent from the APOGEE

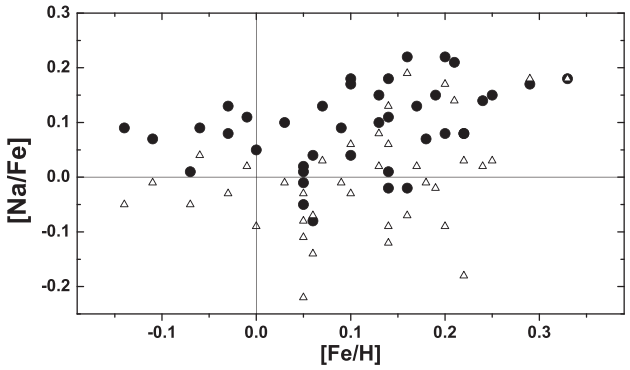

Figure 9. Relative sodium abundances ([Na/Fe] versus [Fe/H] from this analysis (filled circles) compared to the results of analysis Caffau et al. (2019a) (open triangles).

data, although there are some minor differences in the slopes for Na, Mg, and S.

(i) Na. In the upper panel of Fig. 3, [Na/Fe] is plotted as a function of [Fe/H], using Fe as a proxy for metallicity. The four stars with an LTE analysis (open symbols in the figure, connected with a line to the NLTE result) show the small NLTE effects for this parameters space. In fact, of the 12 Na I lines investigated, only three are sensitive to NLTE (see Table A1). In the lower panel of the same figure, Mg is used as a proxy for the metallicity, taking the advantage of a more coherent picture because both Na and Mg are investigated in NLTE. In both panels, a relative increase in the ratio of Na over metallicity at increased metallicity is visible. In Fig. 9, the analysis here done is compared to the analysis by Caffau et al. (2019a) on the same stars. The average difference from the two investigations is 0.09 dex, ranging from about zero to 0.25 dex. This difference is not due to NLTE effects (which is of the order of 0.03 dex), but to the adjustment of the atomic data on the solar spectrum done here and not in Caffau et al. (2019a). Surely with this new analysis the scatter star-to-star is smaller. Summarizing, a great majority of sodium lines in the wide range of effective temperature from 5000 to 6500 K and sodium relative abundances [Na/H] from -0.8 to $+0.8$ are insensitive to the deviation from LTE. This is valid for the dwarfs, but for the stars with log g less than 3 one needs to apply the detailed NLTE calculations.

(ii) Mg. As visible in Fig. 4 and in Table 3, the NLTE effects for Mg are tiny. Of the 26 Mg I lines (the eight components of 1081.1 nm we considered as a single line) investigated, four are sensitive to NLTE (see Table A1). As visible from the Figure, there is an evident trend of the [Mg/Fe] to decreasing at increasing metallicity. In general, in the effective temperature range from 5200 to 6500 K the NLTE effects are the same as previously described (for relative magnesium abundance [Mg/H] from -0.7 to $+0.7$). However, the deviations increase for the giant stars with log g less than 2.5.

(iii) Al. From the upper panel of Fig. 5, one can see a flat [Al/Fe] versus [Fe/H], while on the lower panel, there is a hint for an increasing [Al/Fe] for increasing [Mg/Fe]. The NLTE effects on the Al I lines are about 0.05 dex (see Table 3), smaller than the line-to-line scatter for all stars. The nine Al I lines analysed here suffer all but one from NLTE effects, which are anyway not strong. The mean difference from the analysis of Caffau et al. (2019a) is 0.05 dex, with a few cases with differences up to 0.15 dex that are due to atomic data and line selection. As a concluding remark, it can be noted that two Al I lines 1087.2 and 1089.1 nm can be safely used in LTE analysis for the dwarfs stars with log g larger than 3 and affective temperature lower than 6000 K (for the wide range of the relative aluminium abundances from -0.7 to $+0.7$). At the same time for the subgiant and giant stars, as well as for hotter dwarfs the detailed NLTE calculations are necessary.

(iv) S. In the upper panel of Fig. 6, the decrease of [S/Fe] with increasing metallicity typical in the α-elements, is well evident. In the lower panel of Fig. 6, an almost flat [S/Mg] as a function of [Mg/Fe] as a proxy for metallicity is expected because both Mg and S are α-elements. The behaviour was very similar in Caffau et al. (2019a), also if single stars could differ up to 0.17 dex, due to choice of the lines, atomic data, but also NLTE for the lines belonging to the multiplet 3. 19 lines of S I have been analysed (see Table A1). Only the three lines belonging to the multiplet 3 (the three bluest lines here analysed) are strongly affected by NLTE; the other lines are either well represented in LTE or slightly affected by NLTE. The lines of multiplet 3 are the strongest and sometimes the only possibility to derive A(S) in metal-poor stars. The global NLTE effects on the abundance determination for S is small (up to -0.08, see Table 3) because all the S I lines, but the three of multiplet 3, form in conditions close to LTE. Speaking of sensitivity to atmosphere parameters, one can note that seven S I lines at 2250.7–2270.7 nm show the weak influence from the NLTE effects if we are considering the dwarfs with log g greater than 3 and effective temperatures lower than 6400 K (relative sulphur abundance is from -0.7 to $+0.7$). NLTE effects are becoming remarkable for the subgiant and giant stars. The same is true for the metal-deficient stars ([Fe/H] < -0.7).

(v) K. From both panels of Fig. 7, one can see a decreasing [K/Fe] for increasing metallicity. Of the seven K I lines here analysed, four are affected by NLTE (see Table A1). The NLTE correction for the stars listed in Table 3 is larger than the line-to-line scatter and the large difference of the LTE and NLTE abundance is evident in Fig. 7. The difference with the analysis by Caffau et al. (2019a) is large, certainly affected by the NLTE. Our recommendation for the use of potassium lines depending on the parameters of stellar atmospheres is as follows: lines at 1516.3–1516.8 nm are available for use in the LTE approximation for stars with log $g >$ 3.5 and [K/H] from –0.7 to + 0.7. The effective temperature has almost no effect on the NLTE corrections for these lines.

(vi) Sr. Fig. 8 shows a decrease of [Sr/Fe] or [Sr/Mg] for increasing metallicity. The three lines here analysed are strongly affected by NLTE (see Table A1) and the NLTE corrections for the stars with both LTE and NLTE analysis are much larger than the line-to-line scatter and can be up to 0.45 dex (see Table 3).

Concluding our discussion, we should make the following remark: we recommend using certain IR lines to obtain elemental abundances in LTE, while at the same time leaving open questions about the effect of the limitations of our approach, such as the 1D approximation, on the obtained abundances.

4 CONCLUSION

We analysed IR lines of several ions in the solar spectrum and in the spectra of 40 dwarf stars observed with GIANO spectrograph. We have studied in detail the influence of the NLTE effects on the lines under consideration, and we give our recommendation on which lines can be used to obtain abundance in the LTE approximation, and which lines require NLTE processing. This information is given in the Table A1 in the Appendix.

The sample here discussed is small in size, but has a high quality of the spectra, both in terms of S/N ratio and resolution. It is interesting to note how such a small size sample allows to derive

reliable abundance trends that become apparent only for samples that are several orders of magnitude larger in size, but of lower quality, like the APOGEE sample.

ACKNOWLEDGEMENTS

We would like to thank the referee of this paper for his/her valuable comments.

Based on observations made with GIANO at the Italian Telescopio Nazionale Galileo (TNG) operated on the island of La Palma by the Fundación Galileo Galilei of the INAF (Istituto Nazionale di Astrofisica) at the Spanish Observatorio del Roque de los Muchachos of the Instituto de Astrofisica de Canarias.

REFERENCES

Ahumada R. et al., 2019, preprint (arXiv:1912.02905)
Allende Prieto C. et al., 2008, Astron. Nachr., 329, 1018
Andrievsky S. M., Spite M., Korotin S. A., Spite F., Bonifacio P., Cayrel R., Hill V., François P., 2008, A&A, 481, 481
Andrievsky S. M., Spite M., Korotin S. A., Spite F., Bonifacio P., Cayrel R., François P., Hill V., 2010, A&A, 509, A88
Andrievsky S. M., Spite F., Korotin S. A., François P., Spite M., Bonifacio P., Cayrel R., Hill V., 2011, A&A, 530, A105
Arenou F. et al., 2018, A&A, 616, A17
Barklem P. S., Piskunov N., O'Mara B. J., 2000, A&AS, 142, 467
Belokurov V., Erkal D., Evans N. W., Koposov S. E., Deason A. J., 2018, MNRAS, 478, 611
Belyaev A. K., Yakovleva S. A., 2017, A&A, 606, A147
Biemont E., Quinet P., Zeippen C. J., 1993, A&AS, 102, 435
Butler K., Mendoza C., Zeippen C. J., 1993, J. Phys. B: At. Mol. Opt. Phys., 26, 4409
Caffau E., Ludwig H.-G., Steffen M., Freytag B., Bonifacio P., 2011, Sol. Phys., 268, 255
Caffau E. et al., 2019a, A&A, 622, A68
Caffau E. et al., 2019b, A&A, 628, A46
Carlsson M., 1986, Uppsala Astronomical Observatory Reports, 33
Černiauskas A. et al., 2017, A&A, 604, A35
Chang T. N., Tang X., 1990, J. Quant. Spectrosc. Radiat. Transfer, 43, 207
Cirasuolo M. et al., 2014, in Ramsay S. K., McLean I. S., Takami H., eds, Proc. SPIE Conf. Ser. Vol. 9147, Ground-based and Airborne Instrumentation for Astronomy V. SPIE, Bellingham, p. 91470N
Dalton G. et al., 2018, in Evans C. J., Simard L., Takami H., eds, Proc. SPIE Conf. Ser. Vol. 10702, Ground-based and Airborne Instrumentation for Astronomy VII. SPIE, Bellingham, p. 107021B
de Jong R. S. et al., 2019, Messenger, 175, 3
Di Matteo P., Haywood M., Lehnert M. D., Katz D., Khoperskov S., Snaith O. N., Gómez A., Robichon N., 2019, A&A, 632, A4
Dobrovolskas V. et al., 2014, A&A, 565, A121
Gaia Collaboration, 2018, A&A, 616, A1
Gilmore G. et al., 2012, Messenger, 147, 25
Hase F., Wallace L., McLeod S. D., Harrison J. J., Bernath P. F., 2010, J. Quant. Spectrosc. Radiat. Transfer, 111, 521
Haywood M., Di Matteo P., Lehnert M. D., Snaith O., Khoperskov S., Gómez A., 2018, ApJ, 863, 113
Helmi A., Babusiaux C., Koppelman H. H., Massari D., Veljanoski J., Brown A. G. A., 2018, Nature, 563, 85
Kaeufl H.-U. et al., 2004, in Moorwood A. F. M., Iye M., eds, Proc. SPIE Conf. Ser. Vol. 5492, Ground-based Instrumentation for Astronomy. SPIE, Bellingham, p. 1218
Korotin S. A., 2009, Astron. Rep., 53, 651
Korotin S. A., Mishenina T. V., 1999, Astron. Rep., 43, 533
Korotin S. A., Andrievsky S. M., Luck R. E., 1999, A&A, 351, 168
Kurucz R., 1993, ATLAS9 Stellar Atmosphere Programs and 2 km/s grid. Kurucz CD-ROM No. 13, Mass: Smithsonian Astrophysical Observatory, Cambridge
Kurucz R. L., 2005, Mem. Soc. Astron. Ital. Suppl., 8, 14
Kurucz R. L., Peytremann E., 1975, SAO Special Report, 362
Kurucz R. L., Furenlid I., Brault J., Testerman L., 1984, Solar flux atlas from 296 to 1300 nm, National Solar Observatory, Sunspot, New Mexico
Livingston W., Wallace L., 1991, An atlas of the solar spectrum in infrared from 1850 to 9000 cm-1, NSO Technical Report
McEachran R. P., Cohen M., 1983, J. Phys. B:, 16, 3125
Mishenina T. V., Soubiran C., Kovtyukh V. V., Korotin S. A., 2004, A&A, 418, 551
Nissen P. E., Schuster W. J., 2010, A&A, 511, L10
Nissen P. E., Schuster W. J., 2011, A&A, 530, A15
Origlia L. et al., 2014, Proc. SPIE, 914461E
Quirrenbach A. et al., 2014, in Ramsay S. K., McLean I. S., Takami H., eds, Proc. SPIE Conf. Ser. Vol. 9147, Ground-based and Airborne Instrumentation for Astronomy V. SPIE, Bellingham, p. 91471F
Rayner J. et al., 2016, in Evans C. J., Simard L., Takami H., eds, Proc. SPIE Conf. Ser. Vol. 9908, Ground-based and Airborne Instrumentation for Astronomy VI. SPIE, Bellingham, p. 990884
Reader J., Kramida A., Ralchenko Y., 2012, American Astronomical Society Meeting Abstracts #219, p. 443.01
Reiners A., Mrotzek N., Lemke U., Hinrichs J., Reinsch K., 2016, A&A, 587, A65
Ryabchikova T., Piskunov N., Kurucz R. L., Stempels H. C., Heiter U., Pakhomov Yu, Barklem P. S., 2015, Phys. Scr., 90, 054005
Safronova M. S., Safronova U. I., Clark C. W., 2013, Phys. Rev. A, 87, 052504
Tsymbal V., 1996, in Adelman S. J., Kupka F., Weiss W. W., eds, ASP Conf. Ser. Vol. 108, M.A.S.S., Model Atmospheres and Spectrum Synthesis. Astron. Soc. Pac., San Francisco, p. 198
Unsöld A., 1955, Physik der Stern Atmospharen. Springer, Berlin
Warner B., 1968, MNRAS, 139, 115
Weinberg D. H. et al., 2019, ApJ, 874, 102
Wiese W. L., Smith M. W., Miles B. M., 1969, Atomic Transition Probabilities, Vol. 2. NSRDS-NBS, Washington, D.C.
Zatsarinny O., Tayal S. S., 2010, Phys. Rev. A, 81, 043423

APPENDIX A:

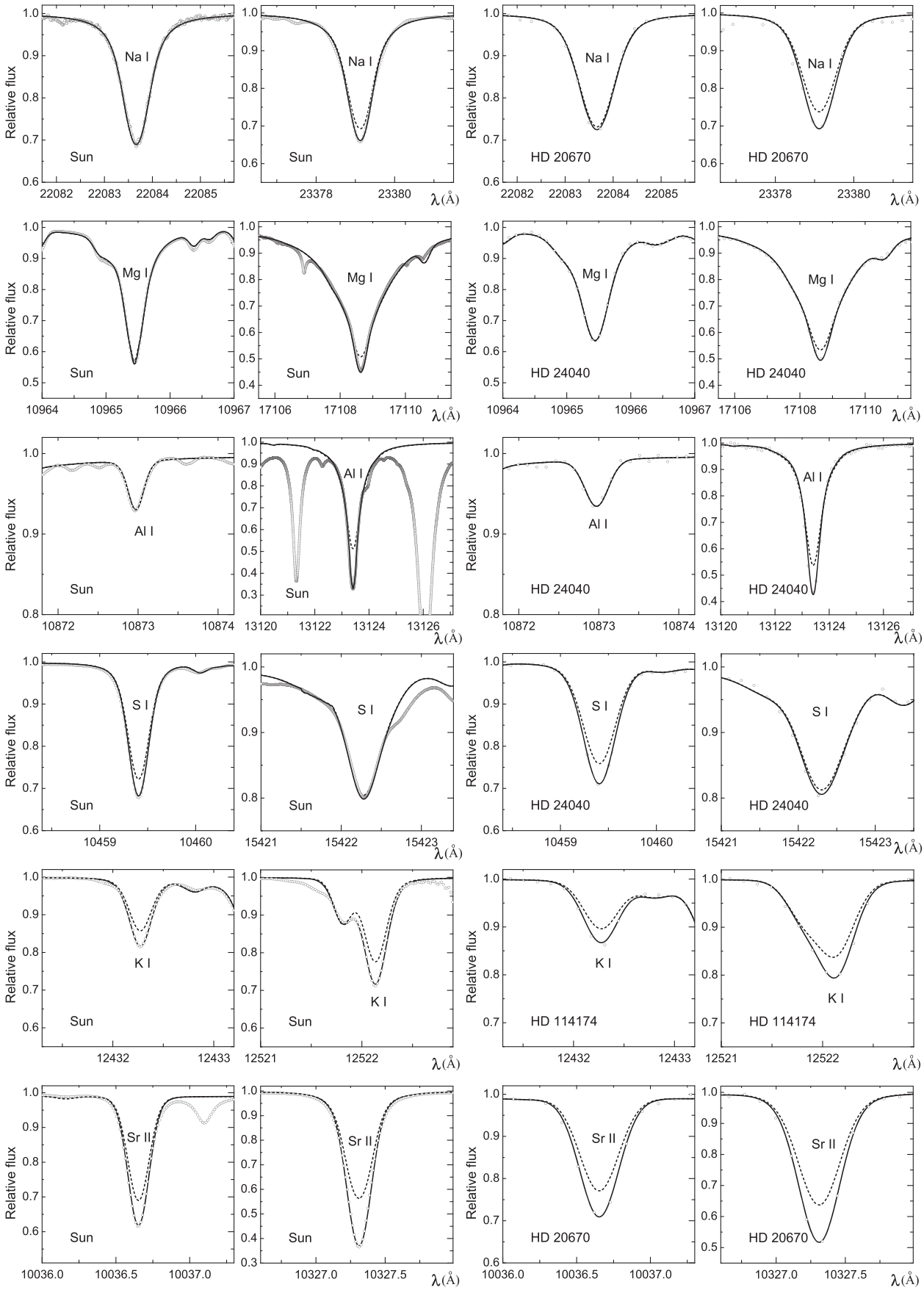

Figure A1. Observed fragments of the spectra (*open circles*) and synthesized profiles of two selected Na I, Mg I, Al I, S I, K I, and Sr II lines. LTE (*dashed line*) and NLTE (*continuous line*).

Table A1. Studied lines and our recommendation: LTE or NLTE.

λ (Å)	log gf	Γ_{vw}	LTE/NLTE	λ (Å)	log gf	Γ_{vw}	LTE/NLTE
Na I				Al I			
10746.45	− 1.29	− 7.06	LTE	10872.97	− 1.33	− 7.19	LTE
10834.85	− 0.50	− 7.06	LTE	10891.74	− 1.03	− 7.19	LTE
10834.85	− 1.80	− 7.06	LTE	13123.41	0.27	− 7.10	NLTE
10834.91	− 0.66	− 7.06	LTE	13150.75	− 0.03	− 7.10	NLTE
12679.17	− 0.04	− 6.65	LTE	16718.96	0.22	− 7.16	NLTE
12679.17	− 1.34	− 6.65	LTE	16750.56	0.47	− 7.16	NLTE
12679.22	− 0.20	− 6.65	LTE	16763.36	− 0.48	− 7.16	small NLTE
22056.40	0.29	− 7.06	LTE	21093.03	− 0.31	− 6.90	NLTE
22083.66	− 0.01	− 7.06	LTE	21163.76	− 0.01	− 6.90	NLTE
23348.38	0.28	− 7.06	NLTE				
23378.96	− 0.42	− 7.06	NLTE	S I			
23379.14	0.54	− 7.06	NLTE	10455.45	0.25	− 7.32	NLTE
				10456.76	− 0.45	− 7.32	NLTE
Mg I				10459.41	0.03	− 7.32	NLTE
9983.19	− 2.15	− 7.01	LTE	15400.08	0.45	− 7.31	small NLTE
9986.48	− 1.68	− 7.01	LTE	15403.72	− 0.28	− 7.31	small NLTE
9993.21	− 1.45	− 7.01	LTE	15403.79	0.63	− 7.31	small NLTE
10811.05	0.02	− 6.82	NLTE	15422.20	− 1.82	− 7.31	small NLTE
10811.08	− 0.14	− 6.82	NLTE	15422.26	− 0.28	− 7.31	small NLTE
10811.10	− 1.04	− 6.82	NLTE	15422.28	0.79	− 7.31	small NLTE
10811.12	− 1.04	− 6.82	NLTE	15469.82	− 0.15	− 7.40	small NLTE
10811.14	− 2.59	− 6.82	NLTE	15475.62	− 0.62	− 7.40	small NLTE
10811.16	− 0.30	− 6.82	NLTE	15478.48	0.08	− 7.40	small NLTE
10811.20	− 0.19	− 6.82	NLTE	22507.56	− 0.48	− 7.61	LTE
10811.22	− 1.28	− 6.82	NLTE	22519.07	− 0.25	− 7.61	LTE
10953.32	− 0.86	− 6.78	LTE	22552.57	− 0.04	− 7.61	LTE
10957.28	− 0.99	− 6.78	LTE	22563.83	− 0.26	− 7.61	LTE
10957.30	− 0.51	− 6.78	LTE	22575.39	− 0.73	− 7.61	LTE
10965.39	− 2.16	− 6.78	LTE	22644.06	− 0.34	− 7.61	LTE
10965.41	− 0.99	− 6.78	LTE	22707.74	0.44	− 7.61	LTE
10965.45	− 0.24	− 6.78	LTE				
11828.17	− 0.33	− 7.19	NLTE	K I			
12039.82	− 1.53	− 7.22	LTE	11769.64	− 0.48	− 7.33	NLTE
12083.28	− 0.79	− 7.12	NLTE	11772.84	0.47	− 7.33	NLTE
12083.65	0.41	− 7.12	NLTE	12432.27	− 0.43	− 7.02	NLTE
12417.94	− 1.66	− 7.15	LTE	12522.13	− 0.13	− 7.02	NLTE
12423.03	− 1.19	− 7.15	LTE	15163.07	0.63	− 7.31	LTE
12433.45	− 0.97	− 7.15	LTE	15163.07	− 0.67	− 7.31	LTE
15025.00	0.36	− 7.05	small NLTE	15168.38	0.48	− 7.31	LTE
15040.25	0.14	− 7.05	small NLTE				
15047.71	− 0.34	− 7.05	small NLTE	Sr II			
15740.71	− 0.21	− 6.95	small NLTE	10036.65	− 1.31	− 7.63	NLTE
15748.89	− 0.34	− 6.95	small NLTE	10327.31	− 0.35	− 7.63	NLTE
15748.99	0.14	− 6.95	small NLTE	10914.88	− 0.64	− 7.63	NLTE
15765.65	− 1.51	− 6.95	small NLTE				
15765.75	− 0.34	− 6.95	small NLTE				
15765.84	0.41	− 6.95	small NLTE				
17108.63	0.06	− 6.98	NLTE				

This paper has been typeset from a TEX/LATEX file prepared by the author.